Single-particle and transport scattering times in narrow GaAs/$Al_xGa_{1-x}As$ quantum wells

U. Bockelmann, G. Abstreiter, and G. Weimann
Walter Schottky Institut, Technische Universität München, D-8046 Garching bei München, Germany

W. Schlapp
Foschungsinstitut der Deutschen Bundespost, D-6100 Darmstadt, Germany
(Received 2 October 1989; revised manuscript received 11 December 1989)

The in-plane motion of electrons in narrow GaAs/$Al_xGa_{1-x}As$ multiple quantum wells is studied experimentally and theoretically as a function of the electron density n_s and the well width L_z. Two characteristic lifetimes—the single-particle relaxation time τ_s and the transport scattering time τ_t—are obtained from magnetotransport measurements. By comparing τ_s and τ_t with detailed calculations, the contributions of interface roughness, remote impurity, and alloy disorder scattering are investigated separately.

Magnetotransport measurements at liquid-helium temperatures are a versatile tool with which to study the electronic properties of two-dimensional systems and they have been widely used in the past.[1] An increasing magnetic field perpendicular to the two-dimensional electron gas (2D EG) changes the electronic density of states, $D(E)$, from being constant to the quasi-zero-dimensional case of discrete broadened Landau levels. The diagonal magnetoconductivity σ_{xx} is caused by disturbing the cyclotron drift motion of the electrons, $V_y=-E_x/B_z$, due to scattering. At low temperatures $\sigma_{xx}\sim D(E_F)$, because only in the vicinity of the Fermi energy E_F do both occupied and unoccupied electronic states exist, which are necessary for elastic scattering. Obviously, σ_{xx} or, alternatively, the magnetoresistivity ρ_{xx} reflects the broadened density of states and therefore contains detailed information about electronic scattering.

We have investigated multiple-quantum-well (MQW) samples which were molecular-beam-epitaxially (MBE) grown on a semi-insulating GaAs(100) substrate and consist of 25–50 individual GaAs quantum wells separated by $Al_{0.35}Ga_{0.65}As$ barriers of typically 50 nm thickness. The central parts (≈ 10 nm) of the barriers are Si doped. A variation in the doping density of three samples and the additional use of the persistent photoeffect result in an experimentally accessible density range from 3.2×10^{11} to 1.4×10^{12} cm^{-2} at a constant L_z of 5.9 nm. Seven samples with different L_z values between 3.7 and 9.5 nm are studied at a constant electron density n_s of 6.5×10^{11} cm^{-2}. All samples are etched in the form of Hall bars, and Ohmic contacts were alloyed to the layers, connecting all the quantum wells in parallel.

ρ_{xx} and ρ_{xy} are measured at temperatures between 0.3 and 6.8 K using a ^{3}He cryomagnetic system. As shown in Fig. 1, all the parallel connected quantum wells exhibit almost the same electron density in the populated ground subband, which results in exactly one observable period of Shubnikov–de Haas (SdH) oscillations. The ρ_{xx} minima and the ρ_{xy} plateaus, which are quite sensitive to inhomogeneity, show only very weak additional structures, even at a temperature of 0.4 K.

From the mobility at zero magnetic field the transport scattering time $\tau_t=m^*/[n_se^2\rho_{xx}(B=0)]$ is obtained using n_s derived from the period of the SdH oscillations. Assuming a single occupied electronic subband at zero temperature and zero magnetic field, the time τ_t is given by[2]

$$\tau_t^{-1}=\frac{m^*}{\pi\hbar^3}\int_0^{\pi}d\vartheta[1-\cos(\vartheta)]|\langle\mathbf{k}|\hat{H}_{\rm def}|\mathbf{k}'\rangle|^2\,, \qquad (1)$$

with $\mathbf{k}'=\mathbf{k}+\mathbf{q}$, $q=2k_F\sin(\vartheta/2)$, and $k_F=\sqrt{2\pi n_s}$.

$|\langle\mathbf{k}|\hat{H}_{\rm def}|\mathbf{k}'\rangle|$ is the probability for scattering by an angle ϑ from a state $\mathbf{k}$ to a state $\mathbf{k}'$ on the Fermi circle due to the scattering Hamiltonian $\hat{H}_{\rm def}$. The contribution of backscattering to the resistance is enhanced compared to small-angle scattering due to the $1-\cos(\vartheta)$ factor in Eq. (1).

On the other hand, all scattering angles contribute

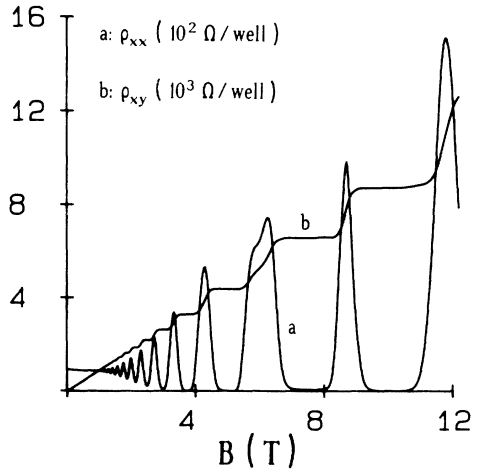

FIG. 1. (a) Shubnikov–de Haas oscillations and (b) quantum Hall effect of a sample consisting of 30 quantum wells with $L_z=9.5$ nm and $n_s=7.2\times10^{11}$ cm^{-2} measured at 0.4 K after illumination.

with equal weight to the broadening $\Gamma=\hbar/2\tau_s$ of single-particle energy levels:[3]

$$\tau_s^{-1}=\frac{m^*}{\pi\hbar^3}\int_0^{\pi}d\vartheta|\langle\mathbf{k}|\hat{H}_{\rm def}|\mathbf{k}'\rangle|^2 . \quad (2)$$

At low magnetic fields, $D(E)$ remains essentially constant with a weak oscillation due to the beginning Landau quantization. The screening and scattering properties are only slightly modified, which suggests that Eq. (2) is still a good approximation and τ_s is independent of the magnetic field in the range where the SdH oscillations are harmonic. This allows the experimental determination of τ_s by the low-magnetic-field dependence of ρ_{xx} at a given temperature T. We obtain τ_s from a fit of the amplitude $\delta\rho$ of ρ_{xx} to

$$\delta\rho\approx C\frac{\xi}{\sinh(\xi)}e^{-\pi/\omega_c\tau_s} , \quad (3)$$

where $\omega_c=eB/m^*$ is the angular cyclotron frequency and $\xi=2\pi^2kT/\hbar\omega_c$. The prefactor C is uncertain due to lack of an exact theoretical description of realistic scatterers in a magnetic field. The present theories[4–6] assume short-range scatterers described by only one lifetime τ. Different relations of τ_t and τ_s to the lifetime τ in the expressions for σ_{xx} and σ_{xy} result in different prefactors C. For the assumption that the classical σ_{xx} and σ_{xy} are controlled by τ_t while the quantum-mechanical deviation thereof is completely characterized by τ_s, we have derived

$$C=4[\omega_c^2\tau_s^2(\omega_c^2\tau_t^2-1+3\tau_t^2\tau_s^{-2})+\tau_t^2\tau_s^{-2}] \times[(1+\omega_c^2\tau_t^2)(1+\omega_c^2\tau_s^2)]^{-1} \quad (4)$$

by taking the quantum-mechanical deviation to linear order.[7] Application of $C\sim B^{-3}$ and $C=4$ according to the Refs. 8 and 9 roughly results in a multiplication of the τ_s values by 0.7 and 1.3, respectively. From our experimental results, no preference for one of the three prefactors C used can be deduced. We observed that the variations of τ_s on different sample parameters are independent of the actual choice of C. The τ_s values published here are obtained by using Eq. (4).

At helium temperatures, where scattering by optical phonons is negligible, one has to consider different competing scattering mechanisms in narrow modulation-doped quantum wells. The individual mechanisms are assumed to be independent of one another, which means that the overall scattering rate is the sum of the individual ones (Matthiesen's rule).

For scattering at charged impurities, one obtains a scattering potential $V^2(q)$,

$$V^2(q)=\left(\frac{2\pi e^2}{q\epsilon_1}\right)^2\int dz\, n_i(z)F^2(q,z) , \quad (5)$$

where ϵ_1 is the static dielectric constant of the lattice, which is assumed to be constant over the whole structure. The density $n_i(z)$ describes the distribution of the impurities in the growth direction z assuming a random distribution in the lateral x-y plane. $F(q,z)$ is the form factor of the effective interaction of an electron in a state $\varphi(z)$ with an impurity at a distance z from the 2D EG:

$$F(q,z)=\int_{-\infty}^{\infty}dz'|\varphi(z')|^2e^{-q|z-z'|} . \quad (6)$$

Interface-roughness (IR) scattering is calculated according to a widely used model after Prange and Nee.[10] The well width is assumed to have lateral deviations $L(\mathbf{r})$ from its target value L_z, with a Gaussian correlation of the form

$$\langle\Delta L(\mathbf{r})\Delta L(\mathbf{r}')\rangle=\Delta^2e^{-|\mathbf{r}-\mathbf{r}'|^2/\Lambda^2} , \quad (7)$$

where Δ can be seen as the mean value and Λ as the average lateral length of the deviation $\Delta L(\mathbf{r})$. By calculating the fluctuations of the energy levels in quantum wells due to the fluctuation of the width according to Eq. (7), one obtains

$$V^2(q)=\frac{\pi^5\hbar^4\Delta^2\Lambda^2}{m^{*2}L_z^6}e^{-q^2\Lambda^2/4}F_{\rm IR}^2 . \quad (8)$$

Gold[11] derived an analytical expression for the form factor $F_{\rm IR}$ which describes the influence of a finite barrier height ($F_{\rm IR}=1$ for infinite barriers, while $F_{\rm IR}$ lies between 0.1 and 0.5 for our samples).

The alloy disorder scattering in the $Al_xGa_{1-x}As$ barriers is described by[2]

$$V^2(q)=\Omega x(1-x)(\Delta V)^2\int_{\rm alloy}dz|\varphi(z)|^4 , \quad (9)$$

where Ω is the volume of the alloy unit cell and ΔV the energy difference of the conduction-band edges of AlAs and GaAs.

The screening of the scattering potentials in Eqs. (5), (8), and (9) by the 2D EG leads to

$$|\langle\mathbf{k}|\hat{H}_{\rm def}|\mathbf{k}'\rangle|^2=\frac{V^2(q)}{\epsilon^2(q)} . \quad (10)$$

We use the static dielectric function $\epsilon(q)$ of the 2D EG in the Lindhart approach including local-field corrections.[3]

The parameters used in the calculations are $m^*/m_0=0.067+0.071x$, $\epsilon_1=12.4$, and $\Delta V=x\times1.04$ eV, where x is the aluminum content and m_0 the mass of the free electron. The average length $\Lambda=6$ nm, in accordance with Ref. 12 and 13, is assumed to be the same for all samples. The wave functions $\varphi(z)$ are calculated analytically,[11] neglecting effects of the self-consistent potential which have only weak influence on the ground subband wave functions. In the doped areas of the $Al_xGa_{1-x}As$ barriers, we assume a constant impurity density $n_i(z)=n_s/l_{\rm dot}$, where $l_{\rm dot}$ is the doped length in the growth direction. For the calculation of remote impurity scattering, we consider the two barriers which enclose a quantum well, neglecting the influence of the other quantum wells.

Figure 2 shows the density dependence of τ_t^{-1} and τ_s^{-1} for the different scattering mechanisms in comparison with our experimental results.

Remote-impurity (RI) scattering (dashed lines) of the 2D EG is mostly via small angles due to the exponential factor in Eq. (6). The suppression of small-angle contributions due to the factor $1-\cos(\vartheta)$ in Eq. (1) compared to Eq. (2) results in the different magnitude and density

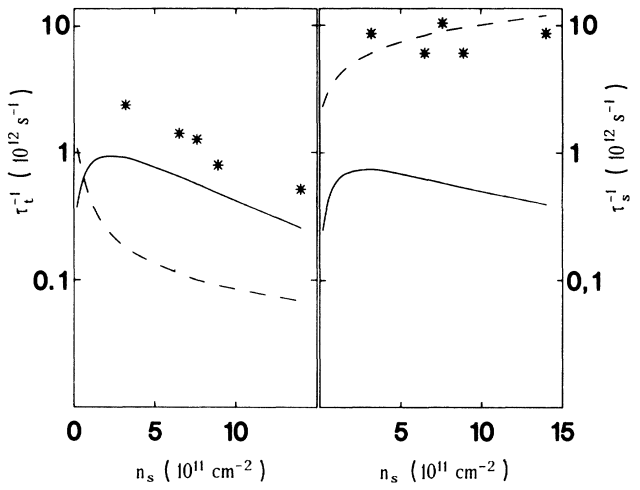

FIG. 2. Scattering rates τ_t^{-1} (left) and τ_s^{-1} (right) for quantum wells with a constant well width L_z of 5.9 nm as a function of carrier concentration n_s. *, experimental results; ——, calculated interface-roughness scattering (assuming $\Delta=2.5$ Å, $\Lambda=60$ Å); — — —, calculated remote-impurity scattering; · · · ·, calculated alloy disorder scattering.

dependence of τ_t and τ_s. The rate τ_s^{-1} for which all scattering angles have equal weight increases with n_s because $n_s \sim n_i(z)$. Nevertheless, τ_t^{-1} decreases because its most important scattering wave vector, $q=2k_F$, increases with n_s while $V^2(q)$ drops exponentially.

Alloy disorder (AD) scattering (dotted lines) is modeled by δ potentials at the lattice sites which are statistically occupied by the Ga and Al atoms. The Fourier transformation of these potentials results in a scattering potential which is independent of q [Eq. (9)]. The 2D EG mainly screens the potential parts which vary slowly in space since $\epsilon(q)$ roughly decreases exponentially with q. Therefore the short-range AD scatters preferentially by large angles, and τ_t is smaller than τ_s.

In the IR model described, the length Λ characterizes the scattering range which has to be compared with the Fermi wavelength $1/k_F$ of the 2D EG. The maxima of the solid lines in Fig. 2 demonstrate the crossover from short- to long-range behavior of IR scattering with increasing n_s. For $k_F\Lambda<1$ the scattering potential is characterized by $\epsilon(q)$, and the scattering rates increase with n_s in analogy to the AD case. The exponential factor in Eq. (8) becomes dominant for $k_F\Lambda>1$, resulting in the decrease of τ_t^{-1} and τ_s^{-1} with increasing n_s. Assuming $\Delta\approx 2.5$ Å, the calculations fit both magnitude and density dependence of our experimental τ_t data. Interface-roughness scattering dominates the transport scattering time for all measured densities n_s. Unfortunately, we are not able to study the range $k_F\Lambda<1$ with the available samples. To observe the predicted maximum in τ_t^{-1} for IR scattering experimentally, the samples should not only have lower densities, but must also have a thicker spacer layer (distance between the 2D EG and the doped region) to avoid the dominance of RI scattering at low densities.

The measured single-particle scattering rates τ_s^{-1} exhibit the magnitude predicted theoretically for RI scattering. The determination of τ_s is sensitive to the individual impurity distribution and the homogeneity of the samples. In particular, the changes caused by varying n_s via the persistent photoconductivity might cause the unsystematic behavior of the experimental τ_s^{-1} plotted versus n_s.

The dependence of the scattering rates on the quantum-well width L_z at a density of 6.5×10^{11} cm^{-2} is shown in Fig. 3. For L_z below 7 nm, the experimental τ_t^{-1} are dominated by IR scattering (solid line).

It is widely assumed that the two interfaces of a quantum well are different because the MBE-grown surface of a binary compound is usually more smooth than that of a ternary alloy. From this point of view, it seems reasonable to attribute the parameter Δ to the roughness of the worse (inverted) interface, assuming the better (normal) interface to be smooth. It is instructive that the values of Δ which fit our experimental results are quite close to the width of 1 monolayer, about 2.8 Å. A real interface, however, is more complex, consisting not only of steps and terraces, but also of charged defects. Therefore, we calculated the scattering at a two-dimensional sheet of impurities located at one boundary of the quantum well (dashed-dotted lines). This model of "interface roughness" does not fit the experimental results well, but it explains the saturation of the decrease of the experimental τ_t^{-1} for $L_z>7$ nm, which cannot be fully attributed to RI scattering (squares) only. The application of an IR model combining both discussed contributions would not influence the results of Fig. 2, but explains better the experimental τ_t data for all L_z.

On the other hand, τ_s is dominated by RI scattering.

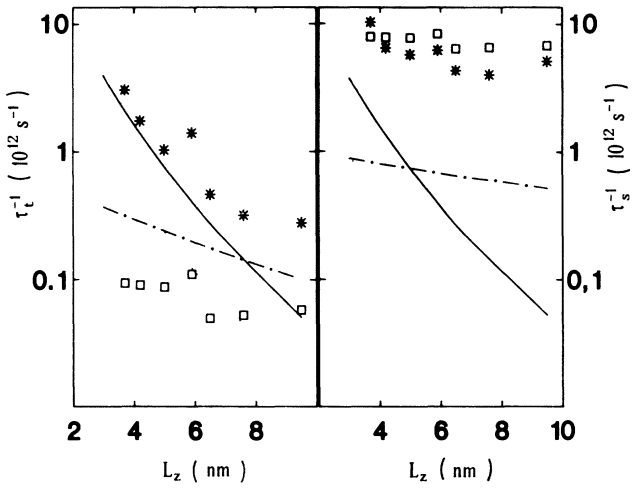

FIG. 3. Scattering rates τ_t^{-1} (left) and τ_s^{-1} (right) for quantum wells with a constant electron density n_s of 6.5×10^{11} cm^{-2} as a function of well width L_z. *, experimental results; ——, calculated interface-roughness scattering (assuming $\Delta=2$ Å, $\Lambda=60$ Å); □, calculated remote-impurity scattering; · · · ·, calculated alloy disorder scattering; –·–, calculated scattering at an impurity sheet with $n_i=2\times10^{10}$ cm^{-2} at one boundary.

Different spacer thicknesses in the different samples cause the discontinuity of both the theoretical RI results and the experimental τ_s^{-1} data plotted versus L_z. The experimental increase of τ_s^{-1} with decreasing L_z below 5 nm shows the contribution of IR scattering.

Comparison of the solid and dashed-dotted lines in Fig. 3 implies that the contribution of IR to the scattering rate τ_t^{-1} (τ_s^{-1}) in our samples is preferably described by the width-fluctuation model for $L_z \lesssim 7$ nm (5 nm) and by the impurity model for $L_z \gtrsim 7$ nm (5 nm), respectively.

Alloy disorder scattering is not dominant in the whole range of n_s and L_z,[11] even under the assumption that the 2D EG is completely unable to screen the δ potentials [$\epsilon(q)=1$].

In conclusion, we have shown that the experimental times τ_s and τ_t which characterize the scattering at zero magnetic field are dominated by remote-impurity and interface-roughness scattering, respectively. The dependences of the experimental data on L_z and n_s are well described by our calculations in the Born approximation.

We want to thank A. Gold, E. Gornik, and R. Küchler for experimental help and stimulating discussions.

[1]T. Ando, A. Fowler, and F. Stern, Rev. Mod. Phys. **54**, 437 (1982).
[2]G. Bastard, *Wave Mechanics Applied to Semiconductor Heterostructures* (Les Editions de Physique, Les Ulis, France, 1988).
[3]A. Gold, Phys. Rev. B **38**, 10 798 (1988).
[4]T. Ando, J. Phys. Soc. Jpn. **37**, 1233 (1974).
[5]T. Ando, Y. Matsumoto, and Y. Uemura, J. Phys. Soc. Jpn. **39**, 279 (1975).
[6]A. Isihara and L. Smrcka, J. Phys. C **19**, 6777 (1986).
[7]U. Bockelmann, P. Hiergeist, G. Abstreiter, G. Weimann, and W. Schlapp, in *Proceedings of the EP2DS8 Conference, Grenoble, 1989* [Surf. Sci. **159** (1990)].
[8]F. F. Fang, T.P. Smith, and S. L. Wright, Surf. Sci. **196**, 310 (1988).
[9]P. T. Coleridge, R. Stoner, and R. Fletcher, Phys. Rev. B **39**, 1120 (1989).
[10]R. E. Prange and T. W. Nee, Phys. Rev. **168**, 779 (1968).
[11]A. Gold, Z. Phys. B **74**, 53 (1989).
[12]H. Sakaki, T. Noda, K. Hirakawa, M. Tanaka, and T. Matsusue, Appl. Phys. Lett. **51**, 1934 (1987).
[13]R. Gottinger, A. Gold, G. Abstreiter, G. Weimann, and W. Schlapp, Europhys. Lett. **6**, 183 (1988).